

FINE-TUNING DISCRETE DIFFUSION MODELS VIA REWARD OPTIMIZATION WITH APPLICATIONS TO DNA AND PROTEIN DESIGN

Anonymous authors

Paper under double-blind review

ABSTRACT

Recent studies have demonstrated the strong empirical performance of diffusion models on discrete sequences (i.e., discrete diffusion models) across domains from natural language to biological sequence generation. For example, in the protein inverse folding task, where the goal is to generate a protein sequence from a given backbone structure, conditional diffusion models have achieved impressive results in generating natural-like sequences that fold back into the original structure. However, practical design tasks often require not only modeling a conditional distribution but also optimizing specific task objectives. For instance, in the inverse folding task, we may prefer protein sequences with high stability. To address this, we consider the scenario where we have pre-trained discrete diffusion models that can generate natural-like sequences, as well as reward models that map sequences to task objectives. We then formulate the reward maximization problem within discrete diffusion models, analogous to reinforcement learning (RL), while minimizing the KL divergence against pretrained diffusion models to preserve naturalness. To solve this RL problem, we propose a novel algorithm, **DRAKES**, that enables direct backpropagation of rewards through entire trajectories generated by diffusion models, by making the originally non-differentiable trajectories differentiable using the Gumbel-Softmax trick. Our theoretical analysis indicates that our approach can generate sequences that are both natural-like (i.e., have a high probability under a pretrained model) and yield high rewards. While similar tasks have been recently explored in diffusion models for continuous domains, our work addresses unique algorithmic and theoretical challenges specific to discrete diffusion models, which arise from their foundation in continuous-time Markov chains rather than Brownian motion. Finally, we demonstrate the effectiveness of our algorithm in generating DNA and protein sequences that optimize enhancer activity and protein stability, respectively, important tasks for gene therapies and protein-based therapeutics.

1 INTRODUCTION

Diffusion models have gained widespread recognition as effective generative models in continuous spaces, such as image and video generation (Song et al., 2020; Ho et al., 2022). Inspired by seminal works (e.g., Austin et al. (2021); Campbell et al. (2022); Sun et al. (2022)), recent studies (Lou et al., 2023; Shi et al., 2024; Sahoo et al., 2024) have shown that diffusion models are also highly effective in discrete spaces, including natural language and biological sequence generation (DNA, RNA, proteins). Unlike autoregressive models commonly used in language modeling, diffusion models are particularly well-suited for biological sequences, where long-range interactions are crucial for the physical behavior of molecules arising from those sequences (e.g., the 3D folded structure of RNA or proteins).

While discrete diffusion models effectively capture conditional distributions (e.g., the distribution of sequences given a specific backbone structure in an inverse protein folding design problem (Dauparas et al., 2022; Campbell et al., 2024)), in many applications, especially for therapeutic discovery, we often aim to generate sequences that are both natural-like and optimize a downstream performance

054
055
056
057
058
059
060
061
062
063
064
065
066
067
068
069
070
071
072
073
074
075
076
077
078
079
080
081
082
083
084
085
086
087
088
089
090
091
092
093
094
095
096
097
098
099
100
101
102
103
104
105
106
107

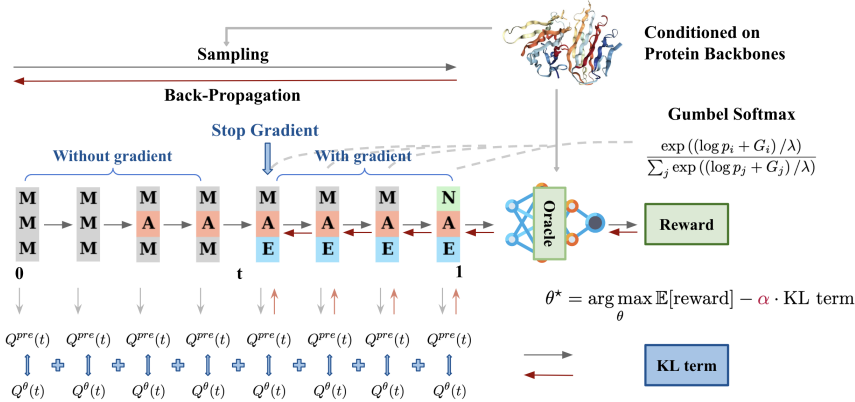


Figure 1: **DRAKES**. We maximize the reward with a penalty term relative to pre-trained discrete diffusion models using the Gumbel-Softmax trick.

objective. For instance, in the inverse folding problem, we may prefer stable protein sequences (i.e., sequences that fold back into stable protein conformations (Widatalla et al., 2024)); for mRNA vaccine production we desire 5’ UTRs that drive high translational efficiency (Castillo-Hair and Seelig, 2021); for gene and cell therapies, we desire regulatory DNA elements, such as promoters and enhancers, that drive high gene expression only in specific cell types (Taskiran et al., 2024); and for natural language we optimize to minimize harmfulness (Touvron et al., 2023).

To address these challenges, our work introduces a fine-tuning approach for well-pretrained discrete diffusion models that maximizes downstream reward functions. Specifically, we aim to optimize these reward functions while ensuring that the generated sequences maintain a high probability under the original conditional distribution (e.g., the distribution of sequences that fold into a given backbone structure). To achieve this, we formulate the problem as a reward maximization task, analogous to reinforcement learning (RL), where the objective function integrates both the reward terms and the KL divergence with respect to the pre-trained discrete diffusion model, which ensures that the generated sequences remain close to the pre-trained model, preserving their naturalness after fine-tuning. To solve this RL problem, we propose a novel algorithm, **DRAKES**, that enables direct backpropagation of rewards through entire trajectories by making the originally non-differentiable trajectories differentiable using the Gumbel-Softmax trick (Jang et al., 2016).

Our main contribution is an RL-based fine-tuning algorithm, Direct Reward backpropagation with gumbel Softmax trick (**DRAKES**), that enables reward-maximizing finetuning for discrete diffusion models (Figure 1). We derive a theoretical guarantee that demonstrates its ability to generate *natural* and *high-reward* designs, and demonstrate its performance empirically on DNA and protein design tasks. While similar algorithms exist for continuous spaces (Fan et al., 2023; Black et al., 2023; Uehara et al., 2024), our work is the first, to the best of our knowledge, to address these aspects in (continuous-time) discrete diffusion models. This requires addressing unique challenges, as discrete diffusion models are formulated as continuous-time Markov chains (CTMC), which differ from Brownian motion, and the induced trajectories from CTMC are no longer differentiable, unlike in continuous spaces. Our novel theoretical guarantee also establishes a connection with recent advancements in classifier guidance for discrete diffusion models (Nisonoff et al., 2024).

2 RELATED WORKS

Discrete diffusion models and their application in biology. Building on the seminal works of Austin et al. (2021); Campbell et al. (2022), recent studies on masked diffusion models (Lou et al., 2023; Shi et al., 2024; Sahoo et al., 2024) have demonstrated strong performance in natural language generation. Recent advances in masked discrete diffusion models have been successfully applied to biological sequence generation, including DNA and protein sequences (Sarkar et al., 2024; Campbell et al., 2024). Compared to autoregressive models, diffusion models may be particularly well-suited for biological sequences, which typically yield molecules that fold into complex three-dimensional (3D) structures.

In contrast to these works, our study focuses on fine-tuning diffusion models to optimize downstream reward functions. One application of our approach is the fine-tuning of protein inverse folding generative models to optimize stability, as discussed in Widatalla et al. (2024). However, unlike this prior work, we employ discrete diffusion models as the generative model.

Controlled generation in diffusion models. There are three primary approaches:

- **Guidance:** Techniques such as classifier guidance (Song et al., 2020; Dhariwal and Nichol, 2021) and its variants (e.g., Bansal et al. (2023); Chung et al. (2022); Ho et al. (2022)) introduce gradients from proxy models during inference. However, since gradients are not formally well-defined for discrete states in diffusion, a recent study (Nisonoff et al., 2024) proposed a method specifically designed for discrete diffusion models. Alternative approaches directly applicable to discrete diffusion models include sequential Monte Carlo (SMC)-based methods (Wu et al., 2024; Trippe et al., 2022; Dou and Song, 2024; Cardoso et al., 2023; Phillips et al., 2024). While these guidance-based inference techniques have their own advantages, they generally lead to longer inference times compared to fine-tuned models. We compare our methods against these in terms of generation quality in Section 6.
- **RL-based fine-tuning:** To maximize reward functions for pretrained diffusion models, numerous recent studies have explored RL-based fine-tuning in continuous diffusion models (i.e., diffusion models for continuous objectives) (Fan et al., 2023; Black et al., 2023; Clark et al., 2023; Prabhudesai et al., 2023). Our work, in contrast, focuses on discrete diffusion models.
- **Classifier-free fine-tuning (Ho and Salimans, 2022):** This approach constructs conditional generative models, applicable in our setting by conditioning on high reward values. Although not originally designed as a fine-tuning method, it can also be adapted for fine-tuning (Zhang et al., 2023) by adding further controls to optimize. However, in the context of continuous diffusion models, compared to RL-based fine-tuning, several works (Uehara et al., 2024) have shown that conditioning on high reward values is suboptimal, because such high-reward samples are rare. We will likewise compare this approach to ours in Section 6. Lastly, when pretrained models are conditional diffusion models (i.e., $p(x|c)$) and the offline dataset size consisting of triplets $(c, x, r(x))$ is limited, it is challenging to achieve success. Indeed, for this reason, most current RL-based fine-tuning papers (e.g., Fan et al. (2023); Black et al. (2023); Clark et al. (2023)) do not empirically compare their algorithms with classifier-free guidance.

3 PRELIMINARY

3.1 DIFFUSION MODELS ON DISCRETE SPACES

In diffusion models, our goal is to model the data distribution $p_{\text{data}} \in \Delta(\mathcal{X})$ using the training data, where \mathcal{X} represents the domain. We focus on the case where $\mathcal{X} = \{1, 2, \dots, N\}$. The fundamental principle is (1) introducing a known forward model that maps the data distribution to a noise distribution, and (2) learning the time reversal that maps the noise distribution back to the data distribution (detailed in Lou et al. (2023); Sahoo et al. (2024); Shi et al. (2024)).

First, we consider the family of distributions $j_t \in \mathbb{R}^N$ (a vector summing to 1) that evolves from $t = 0$ to $t = T$ according to a continuous-time Markov chain (CTMC):

$$\frac{dj_t}{dt} = Q(t)j_t, \quad p_0 \sim p_{\text{data}},$$

where $Q(t) \in \mathbb{R}^{N \times N}$ is the generator. Generally, j_t is designed so that p_t approaches a simple limiting distribution at $t = T$. A common approach is to add *Mask* into \mathcal{X} and gradually mask a sequence so that the limiting distribution becomes completely masked (Shi et al., 2024; Sahoo et al., 2024).

Next, we consider the time-reversal CTMC (Sun et al., 2022) that preserves the marginal distribution. This can be expressed as follows:

$$\frac{dj_{T-t}}{dt} = \bar{Q}(T-t)j_{T-t}, \quad \bar{Q}_{y,x}(t) = \begin{cases} \frac{j_t(y)}{j_t(x)} \bar{Q}_{x,y}(t) & (y \neq x) \\ -\sum_{y \neq x} \bar{Q}_{y,x}(t) & (y = x), \end{cases}$$

where $Q_{y,x}(t)$ is a (y, x) -entry of a generator $Q(t)$. This implies that if we can learn the marginal density ratio $p_t(y)/p_t(x)$, we can sample from the data distribution at $t = T$ by following the above CTMC controlled by $Q(T - t)$. Existing works (e.g., Lou et al. (2023)) demonstrate how to train this ratio from the training data. Especially when we use masked diffusion models (Sahoo et al., 2024; Shi et al., 2024), we get

$$\bar{Q}_{y,x}(t) = \begin{cases} \gamma \mathbb{E}[x_0 = y | x_t = \text{Mask}] & (y \neq \text{Mask}, x_t = \text{Mask}), \\ -\sum_{z \neq \text{Mask}} \gamma \mathbb{E}[x_0 = z | x_t = \text{Mask}] & (y = \text{Mask}, x_t = \text{Mask}) \\ 0 & (x_t \neq \text{Mask}) \end{cases}, \quad (1)$$

for a certain constant γ , where the expectation is taken with respect to (w.r.t.) the distribution induced by the forward CTMC. Notably, the above formulation suggests that masked diffusion models could be viewed as a hierarchical extension of BERT (Devlin, 2018).

Remark 1 (Sequence of multiple tokens). *When dealing with sequences of length M , $x = [x^{(1)}, \dots, x^{(M)}]$, we simply consider the factorized rate matrix, i.e., $\bar{Q}_{y,x} = \sum_i \bar{Q}_{y^{(i)}, x^{(i)}}$ (Campbell et al., 2022), thereby avoiding exponential blowup.*

Remark 2 (Conditioning). *We can easily construct a conditional generative model for any $c \in \mathcal{C}$ by allowing the generator to be a function of $c \in \mathcal{C}$.*

3.2 GOAL: GENERATING NATURAL SAMPLES WHILE OPTIMIZING REWARD FUNCTIONS

In our work, we consider a scenario with a pretrained discrete diffusion model $p^{\text{pre}}(x|c) \in [\mathcal{C} \rightarrow \Delta(\mathcal{X})]$ trained on an extensive dataset and a downstream reward function $r : \mathcal{X} \rightarrow \mathbb{R}$. The pretrained diffusion model captures the naturalness or validity of samples. For example, in protein design, $p^{\text{pre}}(\cdot)$ could be a protein inverse-folding model that generates amino acid sequences that fold back into the given backbone structure (similar to Campbell et al. (2024)), and r could be a function that evaluates stability. Our objective is to fine-tune a generative model to generate *natural-like* samples (high $\log p^{\text{pre}}(\cdot|\cdot)$) with desirable properties (high $r(\cdot)$).

Notation. We introduce a discrete diffusion model parameterized by θ from $t = 0$ to $t = T$:

$$\frac{dp_t}{dt} = Q^\theta(t)p_t, \quad p_0 = p_{\text{lim}}. \quad (2)$$

The parameter θ from the pretrained model is denoted by θ_{pre} . The distribution at time T is denoted as $p^{\text{pre}}(\cdot)$, which approximates the training data distribution p^{data} . We denote an element of the generated trajectory from $t = 0$ to $t = T$ by $x_{0:T}$. For simplicity, we assume the initial distribution is a Dirac delta distribution (completely masked state), and we often treat the original pretrained diffusion model as an unconditional model for a single token for notational convenience. In this paper, all of the proofs are in Appendix C.

4 ALGORITHM

In this section, we present our proposed method, **DRAKES**, for fine-tuning diffusion models to optimize downstream reward functions. We begin by discussing the motivation behind our algorithm.

4.1 KEY FORMULATION

Perhaps the most obvious starting point for fine-tuning diffusion models to maximize a reward function $r(x_T)$ is to simply maximize the expected value of the reward under the model’s distribution, i.e., $\mathbb{E}_{x_0 \sim P^\theta} [r(x_T)]$, where the expectation is taken over the distribution $P^\theta(x_{0:T})$ induced by (2) (i.e., the generator Q^θ). However, using only this objective could lead to over-optimization, where the model produces unrealistic or unnatural samples that technically achieve a high reward, but are impossible to generate in reality. Such samples typically exploit flaws in the reward function, for example, by being outside the training distribution of a learned reward or violating the physical assumptions of a hand-engineered physics-based reward (Levine et al., 2020; Clark et al., 2023; Uehara et al., 2024). We address this challenge by constraining the optimized model to remain close to a pretrained diffusion model, which captures the distribution over natural or realistic samples. More specifically, we introduce a penalization term by incorporating the KL divergence between the fine-tuned model $P^\theta(x_{0:T})$ and the pretrained diffusion model $P^{\theta_{\text{pre}}}(x_{0:T})$ in CTMC.

Accordingly, our goal during fine-tuning is to solve the following reinforcement learning (RL) problem:

$$\theta^* = \operatorname{argmax}_{\theta \in \Theta} \underbrace{\mathbb{E}_{x_{0:T} \sim P^\theta} [r(x_T)]}_{\text{Reward term}} - \underbrace{\alpha \mathbb{E}_{x_{0:T} \sim P^\theta} \left[\int_{t=0}^T \sum_{y \neq x_t} \left\{ Q_{x_t,y}^{\theta_{\text{pre}}}(t) - Q_{x_t,y}^\theta(t) + Q_{x_t,y}^\theta(t) \log \frac{Q_{x_t,y}^\theta(t)}{Q_{x_t,y}^{\theta_{\text{pre}}}(t)} \right\} dt \right]}_{\text{KL term}}. \quad (3)$$

The first term is designed to generate samples with desired properties, while the second term represents the KL divergence. The parameter α controls the strength of this regularization term.

Finally, after fine-tuning, by using the following CTMC from $t = 0$ to $t = T$:

$$\frac{dp_t}{dt} = Q^{\theta^*}(t)p_t, \quad p_0 = p_{\text{lim}}. \quad (4)$$

we generate samples at time T . Interestingly, we can show the following.

Theorem 1 (Fine-Tuned Distribution). *When $\{Q_{\cdot,\cdot}^\theta : \theta \in \Theta\}$ is fully nonparametric (i.e., realizability holds), the generated distribution at time T by (4) is proportional to*

$$\exp(r(\cdot)/\alpha)p^{\text{pre}}(\cdot).$$

This theorem offers valuable insights. The first term, $\exp(r(x))$, represents high rewards. Additionally, the second term, $p^{\text{pre}}(\cdot)$, can be seen as prior information that characterizes the natural sequence. For example, in the context of inverse protein folding, this refers to the ability to fold back into the target backbone structure.

Remark 3. *A similar theorem has been derived for continuous diffusion models (Uehara et al., 2024, Theorem 1). However, our formulation (3) differs significantly as our framework is based on a CTMC, whereas those works are centered around the Brownian motion. Furthermore, while the use of a similar distribution is common in the literature on (autoregressive) large language models (e.g., Ziegler et al. (2019)), its application in discrete diffusion models is novel, considering that $p^{\text{pre}}(\cdot)$ cannot be explicitly obtained in our context, unlike autoregressive models.*

4.2 DIRECT REWARD BACKPROPAGATION WITH GUMBEL SOFTMAX TRICK (DRAKES)

Based on the key formulation presented in Section 4.1, we introduce our proposed method (Algorithm 1 and Figure 1), which is designed to solve the RL problem (3). The core approach involves iteratively (a) sampling from $x_{0:T} \sim P^\theta$ and (b) updating θ by approximating the objective function (3) with its empirical counterpart and adding its gradient with respect to θ into the current θ . Importantly, for step (b) to be valid, step (a) must retain the gradients from θ . After explaining the representation of x_t , we will provide details on each step.

Representation. To represent $x \in \{1, \dots, N\}$, we often use the N -dimensional one-hot encoding representation within \mathbb{R}^N interchangeably. From this perspective, while the original generator corresponds to a map $\mathcal{X} \times \mathcal{X} \rightarrow \mathbb{R}$, we can also regard it as an extended mapping: $\mathbb{R}^N \times \mathbb{R}^N \rightarrow \mathbb{R}$. We will use this extended mapping when we consider our algorithm later.

Stage 1: Data collection (Step 2-9) We aim to sample from the distribution induced by the generator Q^θ . In the standard discretization of CTMC, for $(y, x) \in \mathcal{X} \times \mathcal{X}$, at time t , we use

$$p(x_{t+\Delta t} = y | x_t = x) = \mathbb{I}(x = y) + Q_{y,x}^\theta(t)(\Delta t).$$

Thus, by defining $\pi_t = [Q_{1,x}^\theta(t)(\Delta t), \dots, (1 + Q_{x,x}^\theta(t))\Delta t \dots, Q_{N,x}^\theta(t)(\Delta t)]$, we sample $x_{t+\Delta t} \sim \text{Cat}(\pi_t)$, where $\text{Cat}(\cdot)$ denotes the categorical distribution.

However, this procedure is not differentiable with respect to θ , which limits its applicability for optimization. To address this, we first recognize that sampling from the categorical distribution can be reduced to a Gumbel-max operation. Although this operation itself remains non-differentiable, we can modify it by replacing the max operation with a softmax, as shown in Line 7, which is also utilized in discrete VAE (Jang et al., 2016). This modification results in a new variable, $\bar{x}_t \sim [0, 1]^N$, which maintains differentiability with respect to θ . As the temperature τ approaches zero, \bar{x}_t converges to a sample from the exact categorical distribution $\text{Cat}(\pi_t)$, effectively becoming x_t . Thus, we typically set the temperature to a low value to closely approximate the true distribution.

Algorithm 1 DRAKES (Direct Reward bAcKpropagation with gumbEl Softmax trick)

1: **Require:** Pretrained diffusion models $Q^{\theta_{\text{pre}}} : \mathbb{R}^N \times \mathbb{R}^N \rightarrow \mathbb{R}$, reward $r : \mathcal{X} \rightarrow \mathbb{R}$, learning rate β , Batch size B , Iteration S , Time-step Δt , Temperature τ , Regularization parameter α

2: **for** $s \in [1, \dots, S]$ **do**

3: **for** $i \in [1, \dots, B]$ **do**

4: **for** $t \in [0, \Delta t, \dots, T]$ **do**

5: Set $[\pi(t)_1, \dots, \pi(t)_N] \in \Delta(\mathcal{X})$ where $\pi(t)_y = \begin{cases} [\bar{x}_{t-1}^{(i)}]_y + \Delta t \sum_{x \in \mathcal{X}} [\bar{x}_{t-1}^{(i)}]_x Q_{y,x}^{\theta_s} & (t > 0) \\ p_{\text{lim}}(y) & (t = 0) \end{cases}$

6: Sample $k \in [1, \dots, N]$; $G_k \sim \text{Gumbel}(0, 1)$

7: Set a differentiable counterpart of the sample at time t :

$$\bar{x}_t^{(i)} \leftarrow \left[\frac{\exp((\pi(t)_1 + G_1)/\tau)}{\sum_y \exp((\pi(t)_y + G_y)/\tau)}, \dots, \frac{\exp((\pi(t)_N + G_N)/\tau)}{\sum_y \exp((\pi(t)_y + G_y)/\tau)} \right]$$

8: **end for**

9: **end for**

10: Set the loss:

$$g(\theta_s) = \frac{1}{B} \sum_{i=1}^B \left[r(\bar{x}_T^{(i)}) - \frac{\alpha}{T} \sum_{t=1}^T \sum_{x \in \mathcal{X}} [\bar{x}_{t-1}^{(i)}]_x \sum_{\substack{y \in \mathcal{X} \\ y \neq x}} \left\{ -Q_{x,y}^{\theta_s}(t) + Q_{x,y}^{\theta_{\text{pre}}}(t) + Q_{x,y}^{\theta_s}(t) \log \frac{Q_{x,y}^{\theta_s}(t)}{Q_{x,y}^{\theta_{\text{pre}}}(t)} \right\} \right]$$

11: Update a parameter: $\theta_{s+1} \leftarrow \theta_s + \beta \nabla_{\theta} g(\theta)|_{\theta=\theta_s}$

12: **end for**

13: **Output:** θ_{S+1}

Stage 2: Optimization (Step 10-11) After approximately sampling from the distribution induced by P^{θ_s} , we update the parameter θ_s by maximizing the empirical objective. Although x_t itself may not have a valid gradient, \bar{x}_t retains the gradient with respect to θ . Therefore, we use the empirical approximation based on \bar{x}_t . We offer several remarks below, with details in Appendix D:

- **Validity of \bar{x}_t :** While \bar{x}_t does not strictly belong to \mathcal{X} , this is practically acceptable since the generator $Q^{\theta}(t)$ is parameterized as a map $\mathbb{R}^N \times \mathbb{R}^N \rightarrow \mathbb{R}$.
- **SGD Variants:** Although Line 11 uses the standard SGD update, any off-the-shelf SGD algorithm, such as Adam (Kingma, 2014), can be applied in practice.
- **Soft Calculation with \bar{x}_t :** Transition probability $\pi(t)_y$ and the KL divergence term in $g(\theta)$ are modified to their soft counterparts by using \bar{x}_t in place of x_t .
- **Straight-Through Gumbel Softmax:** Non-relaxed computations can be used in the forward pass (in Line 10). This is commonly known as straight-through Gumbel softmax estimator.
- **Truncated Backpropagation:** In practice, it is often more effective to backpropagate from intermediate time steps rather than starting from $t = 0$. In practice, we adopted this truncation approach, as in Clark et al. (2023).
- **Optimization Objective $g(\theta)$:** For the masked diffusion models (1) that we utilized, $g(\theta)$ can be further simplified to reduce computational complexity, as detailed in Appendix D.2.

5 THEORY OF DRAKES

In this section, we provide an overview of the proof for Theorem 1. Based on the insights gained from this proof, we reinterpret state-of-the-art classifier guidance for discrete diffusion models (Nisonoff et al., 2024) from a new perspective.

5.1 PROOF SKETCH OF THEOREM 1

We define the optimal value function $V_t : \mathcal{X} \rightarrow \mathbb{R}$ as follows:

$$\mathbb{E}_{x_t, T \sim P^{\theta^*}} \left[r(x_T) - \alpha \int_{s=t}^T \sum_{y \neq x_s} \left\{ Q_{x_s, y}^{\theta^*}(s) - Q_{x_s, y}^{\theta_{\text{pre}}}(s) + Q_{x_s, y}^{\theta^*}(s) \log \frac{Q_{x_s, y}^{\theta^*}(s)}{Q_{x_s, y}^{\theta_{\text{pre}}}(s)} \right\} ds \mid x_t = x \right].$$

This represents the expected return when starting from state x at time t and following the optimal policy. Once the optimal value function is defined, the optimal generator can be expressed in terms of this value function, as shown below. This is derived from the Hamilton-Jacobi-Bellman (HJB) equation in CTMC.

Theorem 2 (Optimal generator). *For $x \neq y$ ($x, y \in \mathcal{X}$), we have*

$$Q_{x,y}^{\theta^*}(t) = Q_{x,y}^{\theta_{\text{pre}}}(t) \exp(\{V_t(y) - V_t(x)\}/\alpha).$$

Next, consider an alternative expression for the soft value function, derived using the Kolmogorov backward equations in CTMC. This expression is particularly useful for learning value functions.

Theorem 3 (Feynman–Kac Formula in CTMC).

$$\exp(V_t(x)/\alpha) = \mathbb{E}_{x_t, T \sim P^{\theta_{\text{pre}}}}[\exp(r(x_T)/\alpha) | x_t = x]$$

With this preparation, we can prove our main theorem, which reduces to Theorem 1 when $t = T$.

Theorem 4 (Marginal distribution induced by the optimal generator $Q^{\theta^*}(t)$). *The marginal distribution at time t by (4), $p_t^* \in \Delta(\mathcal{X})$, is proportional to*

$$\exp(V_t(\cdot)/\alpha) p_t^{\text{pre}}(\cdot).$$

where $p_t^{\text{pre}} \in \Delta(\mathcal{X})$ is a marginal distribution induced by pretrained model at t .

This is proved by showing the Kolmogorov forward equation in CTMC: $dp_t^*/dt = Q^{\theta^*}(t)p_t^*$.

5.2 RELATION TO CLASSIFIER GUIDANCE FOR DISCRETE DIFFUSION MODELS

Now, we derive an alternative fine-tuning-free algorithm by leveraging observations in Section 5.1 for reward maximization. If we can directly obtain the optimal generator Q^{θ^*} , we can achieve our objective. Theorem 2 suggests that the optimal generator Q^{θ^*} is a product of the generator from the pretrained model and the value functions. Although we don't know the exact value functions, they can be learned through regression using Theorem 3 based on

$$\exp(V_t(x)/\alpha) = \operatorname{argmin}_{g: \mathcal{X} \rightarrow \mathbb{R}} \mathbb{E}_{x_T \sim P^{\theta_{\text{pre}}}}[\{\exp(r(x_T)/\alpha) - g(x_t)\}^2].$$

In practice, while we can't calculate the exact expectation, we can still replace it with its empirical analog. Alternatively, we can approximate it by using a map from x_t to x_0 in pretrained models following DPS (Chung et al., 2022) or reconstruction guidance (Ho et al., 2022).

Interestingly, a similar algorithm was previously proposed by Nisonoff et al. (2024). While Nisonoff et al. (2024) originally focused on conditional generation, their approach can also be applied to reward maximization or vice versa. In their framework for conditional generation, they define $r(x) = \log p(z|x)$ (e.g., the log-likelihood from a classifier) and set $\alpha = 1$. By adapting Theorem 2 and 3 to their setting, we obtain:

$$Q_{x,y}^{\theta^*}(t) = Q_{x,y}^{\theta_{\text{pre}}}(t) \times p_t(z|y)/p_t(z|x), \quad p_t(z|x_t) := \mathbb{E}_{x_t, T \sim P^{\theta_{\text{pre}}}}[p(z|x_T) | x_t].$$

Thus, we can rederive the formula in Nisonoff et al. (2024).

While this argument suggests that classifier guidance and RL-based fine-tuning approaches theoretically achieve the same goal in an ideal setting (without function approximation, sampling, or optimization errors), their practical behavior can differ significantly, as we demonstrate in Section 6. At a high level, the advantage of classifier guidance is that it requires no fine-tuning, but the inference time may be significantly longer due to the need to recalculate the generator during inference. Indeed, this classifier guidance requires $O(NM)$ computations of value functions at each step to calculate the normalizing constant. While this can be mitigated using a Taylor approximation, there is no theoretical guarantee for this heuristic in discrete diffusion models. Lastly, learning value functions in classifier guidance can often be practically challenging.

6 EXPERIMENTS

Our experiments focus on the design of regulatory DNA sequences for enhancer activity and protein sequences for stability. Our results include comprehensive evaluations, highlighting the ability of **DRAKES** to produce natural-like sequences while effectively optimizing the desired properties.

6.1 BASELINES

We compare **DRAKES** against several baseline methods discussed in Section 2, which we summarize below with further details in Appendix E.1.

- **Guidance-based Methods (CG, SMC, TDS).** We compare our approach with representative guidance-based methods, including state-of-the-art classifier guidance (**CG**) tailored to discrete diffusion models (Nisonoff et al., 2024), SMC-based guidance methods (e.g., Wu et al. (2024)): **SMC**, where the proposal is a pretrained model and **TDS**, where the proposal is CG.
- **Classifier-free Guidance (CFG)** (Ho and Salimans, 2022). CFG is trained on labeled datasets with the measured attributes we aim to optimize.
- **Pretrained.** We generated sequences using pretrained models without fine-tuning.
- **DRAKES w/o KL.** This ablation of **DRAKES** omits the KL regularization term, evaluating how well this term mitigates over-optimization (discussed in Section 4.1).

6.2 REGULATORY DNA SEQUENCE DESIGN

Here we aim to optimize the activity of regulatory DNA sequences such that they drive gene expression in specific cell types, a critical task for cell and gene therapy (Taskiran et al., 2024).

Dataset and settings. We experiment on a publicly available large-scale enhancer dataset (Gosai et al., 2023), which measures the enhancer activity of $\sim 700k$ DNA sequences (200-bp length) in human cell lines using massively parallel reporter assays (MPRAs), where the expression driven by each sequence is measured. We pretrain the masked discrete diffusion model (Sahoo et al., 2024) on all the sequences. We then split the dataset and train two reward oracles (one for finetuning and one for evaluation) on each subset, using the Enformer (Avsec et al., 2021) architecture to predict the activity level in the HepG2 cell line. These datasets and reward models are widely used in the literature on computational enhancer design (Lal et al., 2024; Uehara et al., 2024; Sarkar et al., 2024). Detailed information about the pretrained model and reward oracles is in Appendix E.2.

Evaluations. To comprehensively evaluate each model’s performance in enhancer generation, we use the following metrics:

- *Predicted activity based on the evaluation reward oracle (Pred-Activity).* We predict the enhancer activity level in the HepG2 cell line using the reward oracle trained on the evaluation subset. Note that the diffusion models are fine-tuned (or guided) with the oracle trained on a *different* subset of the data, splitting based on chromosome following conventions (but in the same cell lines) (Lal et al., 2024).
- *Binary classification on chromatin accessibility (ATAC-Acc).* We use an independent binary classification model trained on chromatin accessibility data in the HepG2 cell line (Consortium et al., 2012) (active enhancers should have accessible chromatin). While this is *not* used for fine-tuning, we use it for evaluation to further validate the predicted activity of the synthetic sequences, following Lal et al. (2024).
- *3-mer Pearson correlation (3-mer Corr).* We calculate the 3-mer Pearson correlation between the synthetic sequences and the sequences in the dataset (Gosai et al., 2023) with top 0.1% HepG2 activity level. Models that generate sequences that are more natural-like and in-distribution have a higher correlation.
- *JASPAR motif analysis (JASPAR Corr).* We scan the generated sequences of each model with JASPAR transcription factor binding profiles Castro-Mondragon et al. (2022), which identify potential transcription factor binding motifs in the enhancer sequences (which are expected to drive enhancer activity). We then count the occurrence frequency of each motif and calculate the Spearman correlation of motif frequency between the synthetic sequences generated by each model and the top 0.1% HepG2 activity sequences in the dataset.
- *Log-likelihood of sequences (Log-Lik).* We calculate the log-likelihood of the generated sequences with respect to the pretrained model to measure how likely the sequences are to be natural-like. Models that over-optimize the reward oracle generate out-of-distribution sequences and would have a low likelihood to the pretrained model. The likelihood is calculated using the ELBO of the discrete diffusion model in Sahoo et al. (2024).

Results. **DRAKES** generates sequences with high predicted activity in the HepG2 cell line, as robustly measured by *Pred-Activity* and *ATAC-Acc* (Table 1). The generated sequences closely resemble natural enhancers, as indicated by high 3-mer and JASPAR motif correlations, and a similar likelihood to the pretrained model. These highlight **DRAKES**’s effectiveness in generating plausible high-activity enhancer sequences. Notably, while **DRAKES**, without KL regularization achieves higher *Pred-Activity*, this can be attributed to over-optimization. Despite splitting the data for fine-tuning and evaluation, the sequences remain highly similar due to many analogous regions within each chromosome. However, when evaluated with an independent activity oracle, *ATAC-Acc*, **DRAKES** demonstrates superior performance while maintaining higher correlations and log likelihood.

Table 1: Model performance on regulatory DNA sequence design. **DRAKES** generates sequences with high activity in the HepG2 cell line, measured by *Pred-Activity* and *ATAC-Acc*, while being natural-like by high 3-mer and JASPAR motif correlations and likelihood. We report the mean across 3 random seeds, with standard deviations in parentheses.

Method	Pred-Activity (median) \uparrow	ATAC-Acc \uparrow (%)	3-mer Corr \uparrow	JASPAR Corr \uparrow	Log-Lik (median) \uparrow
Pretrained	0.17(0.04)	1.5(0.2)	-0.061(0.034)	0.249(0.015)	-261(0.6)
CG	3.30(0.00)	0.0(0.0)	-0.065(0.001)	0.212(0.035)	-266(0.6)
SMC	4.15(0.33)	39.9(8.7)	0.840(0.045)	0.756(0.068)	-259(2.5)
TDS	4.64(0.21)	45.3(16.4)	0.848(0.008)	0.846(0.044)	-257(1.5)
CFG	5.04(0.06)	92.1(0.9)	0.746(0.001)	0.864(0.011)	-265(0.6)
DRAKES w/o KL	6.44(0.04)	82.5(2.8)	0.307(0.001)	0.557(0.015)	-281(0.6)
DRAKES	5.61(0.07)	92.5(0.6)	0.887(0.002)	0.911(0.002)	-264(0.6)

6.3 PROTEIN SEQUENCE DESIGN: OPTIMIZING STABILITY IN INVERSE FOLDING MODEL

In this task, given a pretrained inverse folding model that generates sequences conditioned on the backbone’s conformation (3D structure), our goal is to optimize the stability of these generated sequences, following Widatalla et al. (2024).

Dataset and settings. First, we pretrained an inverse folding model based on the diffusion model (Campbell et al., 2024) and the ProteinMPNN (Dauparas et al., 2022) architecture, using the PDB training set from Dauparas et al. (2022). Next, we trained the reward oracles using a different large-scale protein stability dataset, Megascale (Tsuboyama et al., 2023), which includes stability measurements (i.e., the Gibbs free energy change) for ~ 1.8 M sequence variants from 983 natural and designed domains. Following dataset curation and a train-validation-test splitting procedure from Widatalla et al. (2024) (which leads to ~ 0.5 M sequences on 333 domains) and using the ProteinMPNN architecture, we constructed two reward oracles – one for fine-tuning and one for evaluation, that predict stability from the protein sequence and wild-type conformation. Detailed information on the pretrained model and reward oracles is in Appendix E.3.

Evaluations. We use the following metrics to evaluate the stability of the generated sequences and their ability to fold into the desired structure. During evaluation, we always condition on protein backbone conformations from the test data that are *not* used during fine-tuning.

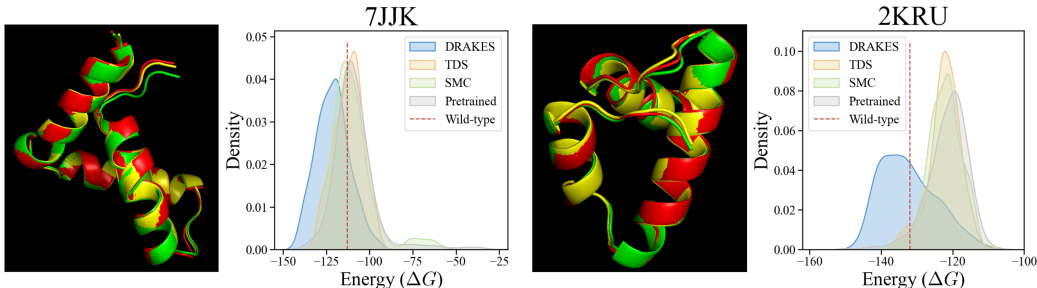
- *Predicted stability on the evaluation reward oracle ($Pred-ddG$).* The evaluation oracle is trained with the full Megascale dataset (train+val+test) to predict protein stability. Conversely, the fine-tuning oracle is trained only with data from the Megascale training set. Thus, during fine-tuning, the algorithms do not encounter any proteins used for evaluation.
- *Self-consistency RMSD of structures ($scRMSD$).* To assess how well a generated sequence folds into the desired structure, we use ESMFold (Lin et al., 2023) to predict the structures of the generated sequences and calculate their RMSD relative to the wild-type structure (i.e., the original backbone structure we are conditioning on). This is a widely used metric (Campbell et al., 2024; Trippe et al., 2022; Chu et al., 2024).

Following prior works (Campbell et al., 2024; Nisonoff et al., 2024), we calculate the success rate of inverse folding as the ratio of generated sequences with $Pred-ddG > 0$ and $scRMSD < 2$.

Results. For inverse protein folding, **DRAKES** generates high-stability protein sequences capable of folding into the conditioned structure (Table 2). It achieves the highest $Pred-ddG$ among all methods,

Table 2: Model performance on inverse protein folding. **DRAKES** generates protein sequences that have high stability and fold to the desired structure, outperforming baselines in the overall success rate. We report the mean across 3 random seeds, with standard deviations in parentheses.

Method	Pred-ddG (median) \uparrow	%(ddG > 0) (%) \uparrow	scRMSD (median) \downarrow	%(scRMSD < 2) (%) \uparrow	Success Rate (%) \uparrow
Pretrained	-0.544(0.037)	36.6(1.0)	0.849(0.013)	90.9(0.6)	34.4(0.5)
CG	-0.561(0.045)	36.9(1.1)	0.839(0.012)	90.9(0.6)	34.7(0.9)
SMC	0.659(0.044)	68.5(3.1)	0.841(0.006)	93.8(0.4)	63.6(4.0)
TDS	0.674(0.086)	68.2(2.4)	0.834(0.001)	94.4(1.2)	62.9(2.8)
CFG	-1.186(0.035)	11.0(0.4)	3.146(0.062)	29.4(1.0)	1.3(0.4)
DRAKES w/o KL	1.108(0.004)	100.0(0.0)	7.307(0.054)	34.1(0.2)	34.1(0.2)
DRAKES	1.095(0.026)	86.4(0.2)	0.918(0.006)	91.8(0.5)	78.6(0.7)



(a) Conditioning on the backbone structure of 7JJK. (b) Conditioning on the backbone structure of 2KRU.

Figure 2: Examples of generated proteins. **Red**: Wild-type backbone structure (the one we condition on), **Yellow**: Structure predicted by ESMFold from the wild-type (true) sequence, **Green**: Structure predicted by ESMFold from the sequence generated by **DRAKES**. The structures for sequences generated by **DRAKES** show good alignment with the original structure (the scRMSDs are 0.768 for 7JJK and 0.492 for 2KRU). Histograms: Gibbs free energy for each generated sequence, calculated using physics-based simulations. In these two cases, the sequences generated by **DRAKES** appear to be more stable than the baselines.

while maintaining a similar success rate of inverse folding (measured by $\%(\text{scRMSD} < 2)$, the percentage of *scRMSD* smaller than 2) as the pretrained model. Considering both factors, **DRAKES** significantly outperforms all baseline methods in terms of overall success rate. Note that CFG does not work well for protein sequence design due to limited labeled data, as Megascale includes only a few hundred backbones, making generalization difficult. This is expected, as we mention in Section 2. Further details are provided in Appendix E.1.

Moreover, the results highlight the importance of the KL term, as **DRAKES** without KL regularization tends to suffer from over-optimization, with high *scRMSD* (i.e., failing to fold back to the target backbone structure), even though *Pred-ddG* may remain high.

In silico validation. For validation purposes, we calculate the stability (i.e., Gibbs free energy) of the generated sequences using physics-based simulations (PyRosetta (Chaudhury et al., 2010)) for wild-type protein backbone structures in Figure 2, following (Widatalla et al., 2024). Although all models are conditioned on the same set of protein backbones, different sets of sequences generated by generative methods can lead to significant differences in side chain interactions, which affect folding energies. The results demonstrate that sequences generated by our algorithms are more stable in this in silico validation compared to other baseline methods. For additional results, refer to Figure 6 in Appendix E.3.

7 CONCLUSIONS

We propose a novel algorithm that incorporates reward maximization into discrete diffusion models, leveraging the Gumbel-Softmax trick to enable differentiable reward backpropagation, and demonstrate its effectiveness in generating DNA and protein sequences optimized for task-specific objectives. For future work, we plan to conduct more extensive in silico validation and pursue wet-lab validation.

540
541
542
543
544
545
546
547
548
549
550
551
552
553
554
555
556
557
558
559
560
561
562
563
564
565
566
567
568
569
570
571
572
573
574
575
576
577
578
579
580
581
582
583
584
585
586
587
588
589
590
591
592
593

REPRODUCIBILITY STATEMENT

For the theoretical results presented in the paper, we provide explanations of assumptions and complete proofs in Appendix C. For the proposed algorithm and experimental results, we provide detailed explanations of the algorithm implementations and experimental setup in Section 4.2, Section 6, Appendix D, and Appendix E, and attach the codes in supplementary materials. For the datasets used in the experiments, we utilize publicly available datasets and elaborate the data processing procedures in Section 6 and Appendix E.

REFERENCES

- 594
595
596 Austin, J., D. D. Johnson, J. Ho, D. Tarlow, and R. Van Den Berg (2021). Structured denoising
597 diffusion models in discrete state-spaces. *Advances in Neural Information Processing Systems 34*,
598 17981–17993.
- 599 Avdeyev, P., C. Shi, Y. Tan, K. Dudnyk, and J. Zhou (2023). Dirichlet diffusion score model for
600 biological sequence generation. *arXiv preprint arXiv:2305.10699*.
- 601
602 Avsec, Ž., V. Agarwal, D. Visentin, J. R. Ledsam, A. Grabska-Barwinska, K. R. Taylor, Y. Assael,
603 J. Jumper, P. Kohli, and D. R. Kelley (2021). Effective gene expression prediction from sequence
604 by integrating long-range interactions. *Nature methods 18*(10), 1196–1203.
- 605 Bansal, A., H.-M. Chu, A. Schwarzschild, S. Sengupta, M. Goldblum, J. Geiping, and T. Goldstein
606 (2023). Universal guidance for diffusion models. In *Proceedings of the IEEE/CVF Conference on*
607 *Computer Vision and Pattern Recognition*, pp. 843–852.
- 608
609 Black, K., M. Janner, Y. Du, I. Kostrikov, and S. Levine (2023). Training diffusion models with
610 reinforcement learning. *arXiv preprint arXiv:2305.13301*.
- 611
612 Campbell, A., J. Benton, V. De Bortoli, T. Rainforth, G. Deligiannidis, and A. Doucet (2022).
613 A continuous time framework for discrete denoising models. *Advances in Neural Information*
614 *Processing Systems 35*, 28266–28279.
- 615
616 Campbell, A., J. Yim, R. Barzilay, T. Rainforth, and T. Jaakkola (2024). Generative flows on discrete
617 state-spaces: Enabling multimodal flows with applications to protein co-design. *arXiv preprint*
arXiv:2402.04997.
- 618
619 Cardoso, G., Y. J. E. Idrissi, S. L. Corff, and E. Moulines (2023). Monte carlo guided diffusion for
620 bayesian linear inverse problems. *arXiv preprint arXiv:2308.07983*.
- 621
622 Castillo-Hair, S. M. and G. Seelig (2021). Machine learning for designing next-generation mrna
623 therapeutics. *Accounts of Chemical Research 55*(1), 24–34.
- 624
625 Castro-Mondragon, J. A., R. Riudavets-Puig, I. Rauluseviciute, R. Berhanu Lemma, L. Turchi,
626 R. Blanc-Mathieu, J. Lucas, P. Boddie, A. Khan, N. Manosalva Pérez, et al. (2022). Jaspas 2022:
627 the 9th release of the open-access database of transcription factor binding profiles. *Nucleic acids*
research 50(D1), D165–D173.
- 628
629 Chaudhury, S., S. Lyskov, and J. J. Gray (2010). Pyrosetta: a script-based interface for implementing
630 molecular modeling algorithms using rosetta. *Bioinformatics 26*(5), 689–691.
- 631
632 Chu, A. E., J. Kim, L. Cheng, G. El Nesr, M. Xu, R. W. Shuai, and P.-S. Huang (2024). An all-atom
633 protein generative model. *Proceedings of the National Academy of Sciences 121*(27), e2311500121.
- 634
635 Chung, H., J. Kim, M. T. Mccann, M. L. Klasky, and J. C. Ye (2022). Diffusion posterior sampling
636 for general noisy inverse problems. *arXiv preprint arXiv:2209.14687*.
- 637
638 Chung, H., B. Sim, D. Ryu, and J. C. Ye (2022). Improving diffusion models for inverse problems
639 using manifold constraints. *Advances in Neural Information Processing Systems 35*, 25683–25696.
- 640
641 Clark, K., P. Vicol, K. Swersky, and D. J. Fleet (2023). Directly fine-tuning diffusion models on
642 differentiable rewards. *arXiv preprint arXiv:2309.17400*.
- 643
644 Consortium, E. P. et al. (2012). An integrated encyclopedia of dna elements in the human genome.
645 *Nature 489*(7414), 57.
- 646
647 Dauparas, J., I. Anishchenko, N. Bennett, H. Bai, R. J. Ragotte, L. F. Milles, B. I. Wicky, A. Courbet,
R. J. de Haas, N. Bethel, et al. (2022). Robust deep learning-based protein sequence design using
proteinmpnn. *Science 378*(6615), 49–56.
- Devlin, J. (2018). Bert: Pre-training of deep bidirectional transformers for language understanding.
arXiv preprint arXiv:1810.04805.

- 648 Dhariwal, P. and A. Nichol (2021). Diffusion models beat gans on image synthesis. *Advances in*
649 *neural information processing systems* 34, 8780–8794.
- 650
- 651 Dou, Z. and Y. Song (2024). Diffusion posterior sampling for linear inverse problem solving: A
652 filtering perspective. In *The Twelfth International Conference on Learning Representations*.
- 653
- 654 Fan, Y., O. Watkins, Y. Du, H. Liu, M. Ryu, C. Boutilier, P. Abbeel, M. Ghavamzadeh, K. Lee, and
655 K. Lee (2023). DPOK: Reinforcement learning for fine-tuning text-to-image diffusion models.
656 *arXiv preprint arXiv:2305.16381*.
- 657 Gosai, S. J., R. I. Castro, N. Fuentes, J. C. Butts, S. Kales, R. R. Noche, K. Mouri, P. C. Sabeti, S. K.
658 Reilly, and R. Tewhey (2023). Machine-guided design of synthetic cell type-specific cis-regulatory
659 elements. *bioRxiv*.
- 660
- 661 Ho, J. and T. Salimans (2022). Classifier-free diffusion guidance. *arXiv preprint arXiv:2207.12598*.
- 662
- 663 Ho, J., T. Salimans, A. Gritsenko, W. Chan, M. Norouzi, and D. J. Fleet (2022). Video diffusion
664 models. *Advances in Neural Information Processing Systems* 35, 8633–8646.
- 665
- 666 Jang, E., S. Gu, and B. Poole (2016). Categorical reparameterization with gumbel-softmax. *arXiv*
preprint arXiv:1611.01144.
- 667
- 668 Kingma, D. P. (2014). Adam: A method for stochastic optimization. *arXiv preprint arXiv:1412.6980*.
- 669
- 670 Lal, A., D. Garfield, T. Biancalani, and G. Eraslan (2024). reglm: Designing realistic regulatory dna
671 with autoregressive language models. *bioRxiv*, 2024–02.
- 672
- 673 Levine, S., A. Kumar, G. Tucker, and J. Fu (2020). Offline reinforcement learning: Tutorial, review,
674 and perspectives on open problems. *arXiv preprint arXiv:2005.01643*.
- 675
- 676 Lin, Z., H. Akin, R. Rao, B. Hie, Z. Zhu, W. Lu, N. Smetanin, R. Verkuil, O. Kabeli, Y. Shmueli, et al.
677 (2023). Evolutionary-scale prediction of atomic-level protein structure with a language model.
Science 379(6637), 1123–1130.
- 678
- 679 Lou, A., C. Meng, and S. Ermon (2023). Discrete diffusion language modeling by estimating the
680 ratios of the data distribution. *arXiv preprint arXiv:2310.16834*.
- 681
- 682 Nisonoff, H., J. Xiong, S. Allenspach, and J. Listgarten (2024). Unlocking guidance for discrete
683 state-space diffusion and flow models. *arXiv preprint arXiv:2406.01572*.
- 684
- 685 Phillips, A., H.-D. Dau, M. J. Hutchinson, V. De Bortoli, G. Deligiannidis, and A. Doucet (2024).
686 Particle denoising diffusion sampler. *arXiv preprint arXiv:2402.06320*.
- 687
- 688 Prabhudesai, M., A. Goyal, D. Pathak, and K. Fragkiadaki (2023). Aligning text-to-image diffusion
689 models with reward backpropagation. *arXiv preprint arXiv:2310.03739*.
- 690
- 691 Sahoo, S. S., M. Arriola, Y. Schiff, A. Gokaslan, E. Marroquin, J. T. Chiu, A. Rush, and V. Kuleshov
692 (2024). Simple and effective masked diffusion language models. *arXiv preprint arXiv:2406.07524*.
- 693
- 694 Sarkar, A., Z. Tang, C. Zhao, and P. Koo (2024). Designing dna with tunable regulatory activity using
695 discrete diffusion. *bioRxiv*, 2024–05.
- 696
- 697 Shi, J., K. Han, Z. Wang, A. Doucet, and M. K. Titsias (2024). Simplified and generalized masked
698 diffusion for discrete data. *arXiv preprint arXiv:2406.04329*.
- 699
- 700 Shi, Y., V. De Bortoli, A. Campbell, and A. Doucet (2024). Diffusion schrödinger bridge matching.
701 *Advances in Neural Information Processing Systems* 36.
- 702
- 703 Song, J., C. Meng, and S. Ermon (2020). Denoising diffusion implicit models. *arXiv preprint*
arXiv:2010.02502.
- 704
- 705 Song, Y., J. Sohl-Dickstein, D. P. Kingma, A. Kumar, S. Ermon, and B. Poole (2020). Score-based
706 generative modeling through stochastic differential equations. *arXiv preprint arXiv:2011.13456*.

- 702 Stark, H., B. Jing, C. Wang, G. Corso, B. Berger, R. Barzilay, and T. Jaakkola (2024). Dirichlet flow
703 matching with applications to dna sequence design. *arXiv preprint arXiv:2402.05841*.
704
- 705 Sun, H., L. Yu, B. Dai, D. Schuurmans, and H. Dai (2022). Score-based continuous-time discrete
706 diffusion models. *arXiv preprint arXiv:2211.16750*.
- 707 Taskiran, I. I., K. I. Spanier, H. Dickmanken, N. Kempynck, A. Panıkova, E. C. Eksi, G. Hulselmans,
708 J. N. Ismail, K. Theunis, R. Vandepoel, et al. (2024). Cell-type-directed design of synthetic
709 enhancers. *Nature* 626(7997), 212–220.
- 710
711 Touvron, H., L. Martin, K. Stone, P. Albert, A. Almahairi, Y. Babaei, N. Bashlykov, S. Batra,
712 P. Bhargava, S. Bhosale, et al. (2023). Llama 2: Open foundation and fine-tuned chat models.
713 *arXiv preprint arXiv:2307.09288*.
- 714 Trippe, B. L., J. Yim, D. Tischer, D. Baker, T. Broderick, R. Barzilay, and T. Jaakkola (2022).
715 Diffusion probabilistic modeling of protein backbones in 3d for the motif-scaffolding problem.
716 *arXiv preprint arXiv:2206.04119*.
- 717
718 Tsuboyama, K., J. Dauparas, J. Chen, E. Laine, Y. Mohseni Behbahani, J. J. Weinstein, N. M. Mangan,
719 S. Ovchinnikov, and G. J. Rocklin (2023). Mega-scale experimental analysis of protein folding
720 stability in biology and design. *Nature* 620(7973), 434–444.
- 721 Uehara, M., Y. Zhao, K. Black, E. Hajiramezanali, G. Scalia, N. L. Diamant, A. M. Tseng, T. Biancalani,
722 and S. Levine (2024). Fine-tuning of continuous-time diffusion models as entropy-
723 regularized control. *arXiv preprint arXiv:2402.15194*.
- 724
725 Uehara, M., Y. Zhao, E. Hajiramezanali, G. Scalia, G. Eraslan, A. Lal, S. Levine, and T. Biancalani
726 (2024). Bridging model-based optimization and generative modeling via conservative fine-tuning
727 of diffusion models. *arXiv preprint arXiv:2405.19673*.
- 728 Widatalla, T., R. Rafailov, and B. Hie (2024). Aligning protein generative models with experimental
729 fitness via direct preference optimization. *bioRxiv*, 2024–05.
- 730
731 Wu, L., B. Trippe, C. Naeseth, D. Blei, and J. P. Cunningham (2024). Practical and asymptotically
732 exact conditional sampling in diffusion models. *Advances in Neural Information Processing
733 Systems* 36.
- 734
735 Yin, G. G. and Q. Zhang (2012). *Continuous-time Markov chains and applications: a singular
736 perturbation approach*, Volume 37. Springer.
- 737
738 Zhang, L., A. Rao, and M. Agrawala (2023). Adding conditional control to text-to-image diffusion
739 models. In *Proceedings of the IEEE/CVF International Conference on Computer Vision*, pp.
740 3836–3847.
- 741
742 Zhou, M., T. Chen, Z. Wang, and H. Zheng (2024). Beta diffusion. *Advances in Neural Information
743 Processing Systems* 36.
- 744
745 Ziegler, D. M., N. Stiennon, J. Wu, T. B. Brown, A. Radford, D. Amodei, P. Christiano, and G. Irving
746 (2019). Fine-tuning language models from human preferences. *arXiv preprint arXiv:1909.08593*.
747
748
749
750
751
752
753
754
755

756 A MORE RELATED WORKS

757
758 **Dirichlet diffusion models for discrete spaces.** Another approach to diffusion models for discrete
759 spaces has been proposed (Stark et al., 2024; Avdeyev et al., 2023; Zhou et al., 2024). In these
760 models, each intermediate state is represented as a vector within a simplex. This is in contrast to
761 masked diffusion models, where each state is a discrete variable.
762

763 B POTENTIAL LIMITATIONS

764
765 We have formulated the RL problem, (3), in the context of CTMC. The proposed algorithm in our
766 paper to solve this problem requires reward models to be differentiable. Since differentiable models
767 are necessary when working with experimental offline data, this assumption is not overly restrictive.
768 Moreover, many state-of-the-art sequence models mapping sequences to functions in genomics are
769 available today. In cases where creating differentiable models is challenging, we recommend using
770 PPO-based algorithms.
771

772 C PROOF OF THEOREMS

773 C.1 PREPARATION

774
775 We prepare two well-known theorems in CTMC for the pedagogic purpose. For example, refer to Yin
776 and Zhang (2012) for the more detailed proof. In these theorems, we suppose we have the CTMC:

$$777 \frac{dp_t}{dt} = Q(t)p_t. \quad (5)$$

778
779 **Lemma 1** (Kolmogorov backward equation). *We consider $g(\cdot, t) = \mathbb{E}[r(x_T)|x_t = \cdot]$ where the
780 expectation is taken w.r.t. (5). Then, this function $g : \mathcal{X} \times [0, T] \rightarrow \mathbb{R}$ is characterized by the
781 following ODE:*

$$782 \frac{dg(x, t)}{dt} = \sum_{y \neq x} Q_{x,y}(t)\{g(x, t) - g(y, t)\}, \quad g(x, T) = r(x_T).$$

783
784 *Proof.* Here, we prove that the p.d.f. g satisfies the above backward equation. To show the converse,
785 we technically require regularity conditions to claim the ODE solution is unique, which can often be
786 proved by the contraction mapping theorem. Here, we skip the converse part.

787
788 When $t = T$, the above statement is obvious. For the rest of the proof, we aim to show a result when
789 $t \neq T$. We have

$$790 g(x_t, t) = \int g(x_{t+dt}, t + dt)p(x_{t+dt}|x_t)dx_{t+dt}.$$

791
792 The above implies

$$793 g(x, t) = \{1 + Q_{x,x}(t)dt\}g(x, t + dt) + \sum_{y \neq x} \{Q_{x,y}(t)dt\}g(y, t + dt).$$

794
795 Now combined with the property of the generator as follows

$$796 0 = \sum_y Q_{x,y}(t + dt),$$

797
798 with some algebra,

$$799 g(x, t) = g(x, t + dt) - \sum_{y \neq x} \{Q_{x,y}(t)dt\}g(x, t + dt) + \sum_{y \neq x} \{Q_{x,y}(t)dt\}g(y, t + dt).$$

800
801 Then, we have

$$802 \frac{g(x, t) - g(x, t + dt)}{dt} = \sum_{y \neq x} Q_{x,y}(t)\{g(y, t + dt) - g(x, t + dt)\}$$

810 Finally, by setting $dt \rightarrow 0$, we obtain

$$811 \quad -\frac{dg(x, t)}{dt} = \sum_{y \neq x} Q_{x,y}(t) \{g(y, t) - g(x, t)\}.$$

814 \square

815
816 **Lemma 2** (Kolmogorov forward equation). *The function $p_t \in \Delta(\mathcal{X})$ is characterized as the following*
817 *ODE:*

$$818 \quad \frac{dp_t(x)}{dt} = \sum_{y \neq x} Q_{y,x}(t)p_t(y) - \sum_{y \neq x} Q_{x,y}(t)p_t(x), \quad p_0 = p_{ini}.$$

819
820
821
822 *Proof.* Here, we prove that the p.d.f. p_t satisfies the above forward equation. To show the converse,
823 we technically require regularity conditions to claim the ODE solution is unique, which can often be
824 proved by the contraction mapping theorem. Here, we skip the converse part.

825 We first have

$$826 \quad p_{t+dt}(x) = \int p_{t+dt}(x|x_t)p_t(x_t)dx_t$$

827
828
829 This implies

$$830 \quad p_{t+dt}(x) = \left\{ \sum_{y \neq x} Q_{y,x}(t)dt p_t(y) \right\} + \{1 + Q_{x,x}(t)dt\}p_t(x)$$

$$831 \quad = \left\{ \sum_{y \neq x} Q_{y,x}(t)dt p_t(y) \right\} + \left\{ 1 - \sum_{y \neq x} Q_{x,y}(t)dt \right\} p_t(x).$$

832
833
834
835 Hence,

$$836 \quad \frac{p_{t+dt}(x) - p_t(x)}{dt} = \left\{ \sum_{y \neq x} Q_{y,x}(t)p_t(y) \right\} - \sum_{y \neq x} Q_{x,y}(t)p_t(x).$$

837
838
839 By taking $dt \rightarrow 0$, we obtain

$$840 \quad \frac{dp_t(x)}{dt} = \sum_{y \neq x} Q_{y,x}(t)p_t(y) - \sum_{y \neq x} Q_{x,y}(t)p_t(x).$$

841
842
843
844 Then, the proof is completed. \square

845 C.2 PROOF OF THEOREM 2

846
847
848 We derive the Hamilton-Jacobi-Bellman (HJB) equation in CTMC. For this purpose, we consider the
849 recursive equation:

$$850 \quad V(x, t) = \max_{\theta} \left[\left\{ \sum_{y \neq x} Q_{x,y}^{\theta}(t) - Q_{x,y}^{\theta_{pre}}(t) - Q_{x,y}^{\theta}(t) \log \frac{Q_{x,y}^{\theta}(t)}{Q_{x,y}^{\theta_{pre}}(t)} \right\} dt \right.$$

$$851 \quad \left. + \sum_{y \neq x} \{Q_{x,y}^{\theta}(t)dt V(y, t + dt)\} + \{1 + Q_{x,x}^{\theta}(t)\}V(x, t + dt) \right].$$

852
853
854 Using $\sum_{y \in \mathcal{X}} Q_{x,y}(t) = 0$, this is equal to

$$855 \quad V(x, t) = \max_{\theta} \left[\left\{ \sum_{y \neq x} Q_{x,y}^{\theta}(t) - Q_{x,y}^{\theta_{pre}}(t) - Q_{x,y}^{\theta}(t) \log \frac{Q_{x,y}^{\theta}(t)}{Q_{x,y}^{\theta_{pre}}(t)} \right\} dt \right.$$

$$856 \quad \left. + V(x, t + dt) + \sum_{y \neq x} Q_{x,y}^{\theta}(t)dt \{V(y, t + dt) - V(x, t + dt)\} \right].$$

By taking dt to 0, the above is equal to

$$-\frac{dV(x,t)}{dt} = \max_{\theta \in \Theta} \left\{ \left[\sum_{y \neq x} Q_{x,y}^{\theta}(t) - Q_{x,y}^{\theta_{\text{pre}}}(t) - Q_{x,y}^{\theta}(t) \log \frac{Q_{x,y}^{\theta}(t)}{Q_{x,y}^{\theta_{\text{pre}}}(t)} \right] + \sum_{y \neq x} Q_{x,y}^{\theta}(t) \{V(y,t) - V(x,t)\} \right\} \quad (6)$$

This is the HBJ equation in CTMC.

Finally, with simple algebra (i.e., taking functional derivative under the constraint $0 = \sum_{y \in \mathcal{X}} Q_{x,y}^{\theta}(t)$), we can show

$$\forall x \neq y; Q_{x,y}^{\theta^*}(t) = Q_{x,y}^{\theta_{\text{pre}}}(t) \exp(\{V(y,t) - V(x,t)\}).$$

C.3 PROOF OF THEOREM 3

This theorem is proved by invoking the Kolmogorov backward equation.

First, by plugging

$$\forall x \neq y; Q_{x,y}^{\theta^*}(t) = Q_{x,y}^{\theta_{\text{pre}}}(t) \exp(\{V(y,t) - V(x,t)\}).$$

into (6), we get

$$\frac{dV(x,t)}{dt} = \sum_{y \neq x} Q_{x,y}^{\theta_{\text{pre}}}(t) \{1 - \exp(\{V(y,t) - V(x,t)\})\}.$$

By multiplying $\exp(V(x,t))$ to both sides, it reduces to

$$\frac{d \exp(V(x,t))}{dt} = \sum_{y \neq x} Q_{x,y}^{\theta_{\text{pre}}}(t) \{\exp(V(x,t)) - \exp(V(y,t))\}. \quad (7)$$

Furthermore, clearly, $V(x,T) = r(x_T)$. Then, the statement is proved by invoking the Kolmogorov backward equation.

C.4 PROOF OF THEOREM 4

We define

$$H_t(x) := \exp(V(x,t)) p_t(x) / C.$$

We aim to prove that the above satisfies the Kolmogorov forward equation:

$$\underbrace{\frac{dH_t(x)}{dt}}_{\text{l.h.s.}} = \underbrace{\sum_{y \neq x} Q_{y,x}^{\theta^*}(t) H_t(y) - \sum_{y \neq x} Q_{x,y}^{\theta^*}(t) H_t(x)}_{\text{r.h.s.}}, \quad p_{ini} = H_0(\cdot).$$

First, we calculate the l.h.s. Here, recall

$$\frac{d \exp(V(x,t))}{dt} = \sum_{y \neq x} Q_{x,y}^{\theta_{\text{pre}}}(t) \{\exp(V(x,t)) - \exp(V(y,t))\}$$

using (7), and

$$\frac{dp_t(x)}{dt} = \sum_{y \neq x} Q_{y,x}^{\theta_{\text{pre}}}(t) p_t(y) - \sum_{y \neq x} Q_{x,y}^{\theta_{\text{pre}}}(t) p_t(x)$$

holds, using the Kolmogorov forward equation. Then, we obtain

$$\begin{aligned}
\frac{dH_t(x)}{dt} &= \frac{1}{C} \times \left\{ \frac{d \exp(V(x, t))}{dt} p_t(x) + \exp(V(x, t)) \frac{dp_t(x)}{dt} \right\} \\
&= \frac{1}{C} \times \left[\sum_{y \neq x} Q_{x,y}^{\theta_{\text{pre}}}(t) \{ \exp(V(x, t)) - \exp(V(y, t)) \} p_t(x) \right] \\
&\quad + \frac{1}{C} \times \exp(V(x, t)) \left\{ \sum_{y \neq x} Q_{y,x}^{\theta_{\text{pre}}}(t) p_t(y) - \sum_{y \neq x} Q_{x,y}^{\theta_{\text{pre}}}(t) p_t(x) \right\} \\
&= \frac{1}{C} \times \sum_{y \neq x} Q_{y,x}^{\theta_{\text{pre}}}(t) \exp(V(x, t)) p_t(y) - \frac{1}{C} \times \sum_{y \neq x} Q_{x,y}^{\theta_{\text{pre}}}(t) \exp(V(y, t)) p_t(x).
\end{aligned}$$

On the other hand, the r.h.s. is

$$\begin{aligned}
&\frac{1}{C} \times \left\{ \sum_{y \neq x} Q_{y,x}^{\theta^*}(t) H_t(y) - \sum_{y \neq x} Q_{x,y}^{\theta^*}(t) H_t(x) \right\} \\
&= \frac{1}{C} \times \sum_{y \neq x} Q_{y,x}^{\theta_{\text{pre}}}(t) \exp(\{V(x, t) - V(y, t)\}) H_t(y) - \frac{1}{C} \sum_{y \neq x} Q_{x,y}^{\theta_{\text{pre}}}(t) \exp(\{V(y, t) - V(x, t)\}) H_t(x) \\
&= \frac{1}{C} \times \sum_{y \neq x} Q_{y,x}^{\theta_{\text{pre}}}(t) \exp(V(x, t)) p_t(y) - \frac{1}{C} \times \sum_{y \neq x} Q_{x,y}^{\theta_{\text{pre}}}(t) \exp(V(y, t)) p_t(x).
\end{aligned}$$

Here, from the first line to the second line, we use

$$\forall x \neq y; Q_{x,y}^{\theta^*}(t) = Q_{x,y}^{\theta_{\text{pre}}}(t) \exp(\{V(y, t) - V(x, t)\}).$$

Finally, we can see that $l.h.s. = r.h.s.$ Furthermore, recalling we have an assumption that p_{ini} is Dirac delta distribution, we clearly have $p_{ini} = H_0(\cdot)$. Hence, the statement is proved by the Kolmogorov forward equation.

D DETAILS OF ALGORITHM

D.1 STRAIGHT-THROUGH GUMBEL SOFTMAX

We apply the straight-through Gumbel softmax estimator to the last time step, i.e.

$$\text{ST}(x_T^{(i)}) := \bar{x}_T^{(i)} + \text{SG}(x_T^{(i)} - \bar{x}_T^{(i)})$$

where $x_T^{(i)}$ is the corresponding Gumbel-max variable, i.e. $x_T^{(i)} = \operatorname{argmax}_{x \in \mathcal{X}} [\bar{x}_T^{(i)}]_x$, and SG denotes stop gradient. Then, $\text{ST}(x_T^{(i)})$ is input into the reward function $r(\cdot)$ instead of $\bar{x}_T^{(i)}$ for forward and backward propagation.

We observe a boost in fine-tuning performance with the straight-through Gumbel softmax, as converting the input to $r(\cdot)$ into a one-hot vector makes it better aligned with the reward oracle’s training distribution.

D.2 SIMPLIFIED FORMULA OF $g(\theta)$

The key objective function in **DRAKES**, $g(\theta)$, can be further simplified for the masked diffusion models that we utilized in the experiments.

$$g(\theta) = \frac{1}{B} \sum_{i=1}^B \left[r(\bar{x}_T^{(i)}) - \frac{\alpha}{T} \sum_{t=1}^T \sum_{x \in \mathcal{X}} [\bar{x}_{t-1}^{(i)}]_x \sum_{\substack{y \in \mathcal{X} \\ y \neq x}} \left\{ -Q_{x,y}^{\theta}(t) + Q_{x,y}^{\theta_{\text{pre}}}(t) + Q_{x,y}^{\theta}(t) \log \frac{Q_{x,y}^{\theta}(t)}{Q_{x,y}^{\theta_{\text{pre}}}(t)} \right\} \right]$$

We denote the second term estimating the KL divergence with the i -th sample as $k_i(\theta)$:

$$k^{(i)}(\theta) = \frac{1}{T} \sum_{t=1}^T \sum_{x \in \mathcal{X}} [\bar{x}_{t-1}^{(i)}]_x \sum_{\substack{y \in \mathcal{X} \\ y \neq x}} \left\{ -Q_{x,y}^\theta(t) + Q_{x,y}^{\theta_{\text{pre}}}(t) + Q_{x,y}^\theta(t) \log \frac{Q_{x,y}^\theta(t)}{Q_{x,y}^{\theta_{\text{pre}}}(t)} \right\}$$

When $x = \text{Mask}$, the value of $Q_{x,y}(t)$ is irrelevant to the parametrization θ , i.e.

$$Q_{x,y}^\theta(t) = Q_{x,y}^{\theta_{\text{pre}}}(t) = \begin{cases} 0, & y \neq \text{Mask} \\ -\gamma, & y = \text{Mask} \end{cases}$$

where γ is a constant related to the forward process schedule (Sahoo et al., 2024). In particular, when applying a linear schedule (as in our experiments), $\gamma = 1/t$. Thus, the corresponding KL divergence component equals 0.

When $x \neq \text{Mask}$,

$$Q_{x,y}^\theta(t) = \begin{cases} 0, & y \neq \text{Mask} \\ \gamma \mathbb{E}_\theta[x_0 = x | x_{t-1} = \text{Mask}], & y = \text{Mask} \end{cases}$$

Denote $\mathbb{E}_\theta[x_0 = x | x_{t-1} = \text{Mask}]$ as $[\hat{x}_0^\theta]_x$. The KL divergence term $k^{(i)}(\theta)$ can be simplified as

$$\begin{aligned} k^{(i)}(\theta) &= \frac{1}{T} \sum_{t=1}^T \sum_{x \in \mathcal{X}} [\bar{x}_{t-1}^{(i)}]_x \sum_{\substack{y \in \mathcal{X} \\ y \neq x}} \left\{ -Q_{x,y}^\theta(t) + Q_{x,y}^{\theta_{\text{pre}}}(t) + Q_{x,y}^\theta(t) \log \frac{Q_{x,y}^\theta(t)}{Q_{x,y}^{\theta_{\text{pre}}}(t)} \right\} \\ &= \frac{1}{T} \sum_{t=1}^T \sum_{x \in \mathcal{X}} [\bar{x}_{t-1}^{(i)}]_x \left\{ -Q_{x,\text{Mask}}^\theta(t) + Q_{x,\text{Mask}}^{\theta_{\text{pre}}}(t) + Q_{x,\text{Mask}}^\theta(t) \log \frac{Q_{x,\text{Mask}}^\theta(t)}{Q_{x,\text{Mask}}^{\theta_{\text{pre}}}(t)} \right\} \\ &= \frac{\gamma}{T} \sum_{t=1}^T \sum_{\substack{x \in \mathcal{X} \\ x \neq \text{Mask}}} [\bar{x}_{t-1}^{(i)}]_x \left\{ -[\hat{x}_0^\theta]_x + [\hat{x}_0^{\theta_{\text{pre}}}]_x + [\hat{x}_0^\theta]_x \log \frac{[\hat{x}_0^\theta]_x}{[\hat{x}_0^{\theta_{\text{pre}}}]_x} \right\} \end{aligned}$$

The simplified formula reduces the computational complexity of calculating $k^{(i)}(\theta)$ to $O(NT)$.

D.3 SCHEDULE OF GUMBEL SOFTMAX TEMPERATURE

We use a linear schedule for the Gumbel softmax temperature τ , decreasing over time as $\tau \sim 1/t$. In early time steps, the temperature is higher, introducing more uncertainty, while later steps have a lower temperature, approximating the true distribution more closely. This improves the fine-tuning procedure as the input becomes closer to clean data at later time steps and the uncertainty of model prediction is reduced.

E EXPERIMENTAL DETAILS AND ADDITIONAL RESULTS

E.1 BASELINES

In this section, we provide a detailed overview of each baseline method.

- **Guidance-based Methods.** Guidance-based methods are based on the pretrained model while adjusting during the sampling process according to the targeted property. This leads to longer inference time compared to fine-tuning approaches.
 - **CG** (Nisonoff et al., 2024). CG adjusts the transition rate of CTMC by calculating the predictor guidance:

$$Q_{x,y|r}(t) = \frac{p(r|y, t)}{p(r|x, t)} Q_{x,y}(t)$$

where r is the target property, and the predictor guidance is further approximated using a Taylor expansion, i.e.

$$\log \frac{p(r|y, t)}{p(r|x, t)} \approx (y - x)^T \nabla_x \log p(r|x, t)$$

The predictor $p(r|x, t)$ is estimated using the posterior mean approach (Chung et al., 2022), where the pretrained model is first utilized to estimate the clean data from the noisy input x_t , and then the reward oracle is applied to the predicted clean sequence. We remark that the above Taylor approximation doesn’t have formal theoretical guarantees, considering that x is discrete. This could be a reason why it does not work well in the case of protein-inverse folding in Section 6.3.

- **SMC** (Wu et al., 2024). SMC is a sequential Monte Carlo-based approach that uses the pretrained model as the proposal distribution. While it was originally designed for conditioning rather than reward maximization, it can be adapted for reward maximization by treating rewards as classifiers. In our experiment, we use this adapted version.
- **TDS** (Wu et al., 2024). Similar to SMC, TDS also applies sequential Monte Carlo, but utilizes CG rather than the pretrained model as the proposal.
- **Classifier-free Guidance (CFG)** (Ho and Salimans, 2022). Unlike guidance-based methods, CFG trains a conditional generative model from scratch and does not rely on the pretrained model. To generate sequences x with desired properties $r(x)$, CFG incorporates $r(x)$ as an additional input to the diffusion model and generates samples conditioning on high $r(x)$ values. Specifically, binary labels of $r(x)$ are constructed according to the 95% quantile, and sampling is done conditioned on the label corresponding to high values of $r(x)$.

It is important to note that CFG requires labeled data pairs $\{x, r(x)\}$ for training, which can limit its performance in cases with limited labeled data, especially when the pretrained model is already a conditional diffusion model $p(x|c)$. For example, in the protein inverse folding task, where x is the protein sequence, c is the protein structure, and $r(x)$ is the protein stability, CFG struggles, as shown in Table 2. This is due to the small size of the Megascale dataset (containing only a few hundred different protein structures), which reduces its capability and generalizability¹. While data augmentation can be applied to construct additional training data, it is resource-intensive, requires significant case-by-case design, and is beyond the scope of this work. For the DNA sequence design task, since all sequences in the dataset are labeled, there is no such issue.

E.2 REGULATORY DNA SEQUENCE DESIGN

Reward Oracle. We train reward oracles to predict activity levels of enhancers in the HepG2 cell line using the dataset from Gosai et al. (2023). Following standard practice (Lal et al., 2024), we split the dataset into two subsets based on chromosomes, with each containing enhancers from half of the 23 human chromosomes. We train two reward oracles on each subset independently using the Enformer (Avsec et al., 2021) architecture initialized with its pretrained weights. One oracle is used for fine-tuning, while the other is reserved for evaluation (i.e. *Pred-Activity* in Table 1). Denote the subset used for training the fine-tuning oracle as FT and the subset for training the evaluation oracle as Eval. Table 3 presents the model performance for both oracles on each subset. Both oracles perform similarly, achieving a high Pearson correlation (> 0.85) on their respective held-out sets (Eval for the fine-tuning oracle and FT for the evaluation oracle).

Table 3: Performance of the reward oracles for predicting HepG2 activity of enhancer sequences.

Model	Eval Dataset	MSE ↓	Pearson Corr ↑
Fine-Tuning Oracle	FT	0.149	0.938
	Eval	0.360	0.869
Evaluation Oracle	FT	0.332	0.852
	Eval	0.161	0.941

¹In contrast, other methods (guidance-based methods and fine-tuning methods) leverage the pretrained model trained on the much larger PDB dataset ($\sim 23,000$ structures) and achieve better performance.

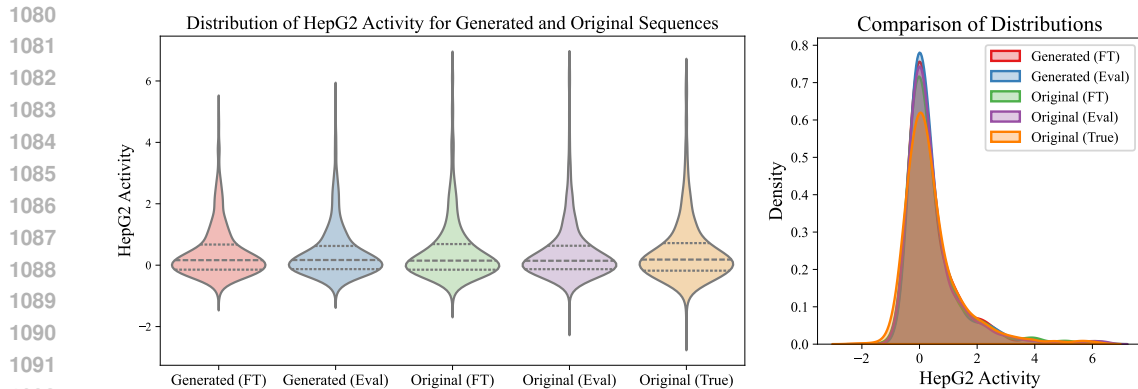


Figure 3: Comparison of HepG2 activity distributions between original sequences and those generated by the pretrained model. The activity distributions match closely with each other.

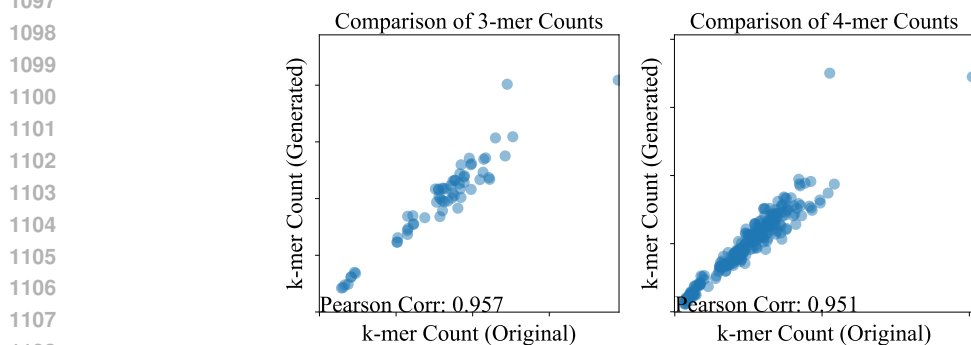


Figure 4: 3-mer and 4-mer Pearson correlation between the original and generated sequences.

Pretrained Model. We pretrain the masked discrete diffusion model (Sahoo et al., 2024) on the full dataset of Gosai et al. (2023), using the same CNN architecture as in Stark et al. (2024) and a linear noise schedule. Other hyperparameters are kept identical to those in Sahoo et al. (2024). To assess the model’s ability to generate realistic enhancer sequences, we sample 1280 sequences and compare them with 1280 randomly selected sequences from the original dataset. Figure 3 presents the distribution of HepG2 activity predicted by either the fine-tuning (FT) or evaluation (Eval) oracle for both the generated and original sequences, along with the true observations for the original sequences. The activity levels of the generated sequences align well with those of the original dataset, indicating the effectiveness of pretrained model in generating in-distribution enhancer sequences. Furthermore, Figure 4 shows the 3-mer and 4-mer Pearson correlation between the synthetic and original sequences, both of which exceed 0.95, further validating the model’s performance.

Fine-tuning Setup. We utilize the pretrained masked discrete diffusion model and the fine-tuning oracle described above for fine-tuning. During **DRAKES**’s stage 1 data collection, sequences are generated from the pretrained model over 128 steps. We set $\alpha = 0.001$ to govern the strength of the KL regularization and truncate the backpropagation at step 50. The model is fine-tuned with 128 samples as a batch (32 samples per iteration, with gradient accumulated over 4 iterations) for 1000 steps. For **DRAKES** w/o KL, we follow the same setup, but set α to zero. For evaluation, we generate 640 sequences per method (with batch size of 64 over 10 batches) for each random seed. We report the mean and standard deviation of model performance across 3 random seeds.

Additional Results for Fine-Tuning. Along with the median Pred-Activity values shown in Table 1, Figure 5 presents the full distribution of Pred-Activity for each method, which shows consistent patterns as Table 1.

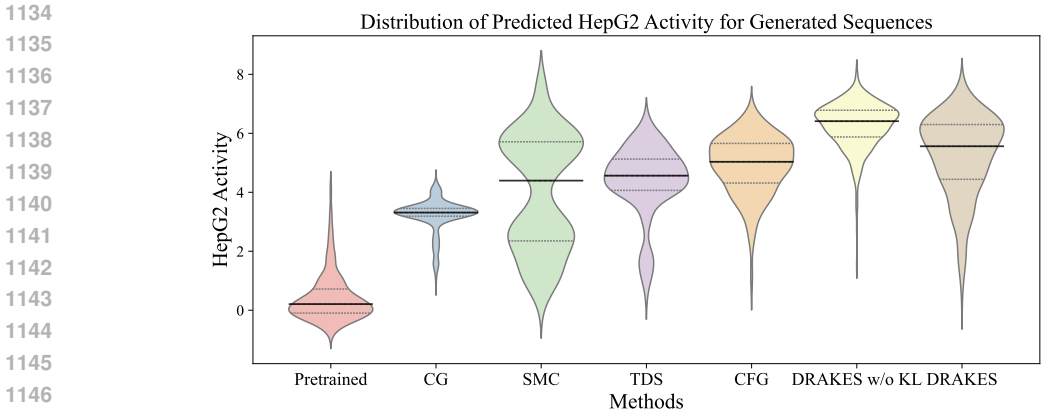


Figure 5: Distribution of Pred-Activity for the generated sequences of each method.

E.3 PROTEIN INVERSE FOLDING

Dataset Curation. We utilize the large-scale protein stability dataset, Megascale (Tsuboyama et al., 2023) for the protein inverse folding experiment, which contains stability measurements for $\sim 1.8M$ sequence variants (for example, single mutants and double mutants) from 983 protein domains. We follow the dataset curation and train-validation-test splitting procedure from Widatalla et al. (2024). Specifically, the wild-type protein structures are clustered with Foldseek clustering and the data is split based on clusters. We then drop a few proteins with ambiguous wild type labels, and clip the ΔG values that are outside the dynamic range of the experiment (> 5 or < 1) to the closest measurable value (5 or 1) as in Nisonoff et al. (2024). We further exclude proteins where a significant proportion of the corresponding variants’ ΔG measurements fall outside the experimental range. The final dataset consists of 438,540 sequence variants from 311 proteins in the training set, 15,182 sequences from 10 proteins in the validation set, and 23,466 sequences from 12 proteins in the test set.

Pretrained Model. We pretrain an inverse folding model using the discrete flow model loss from (Campbell et al., 2024) and the ProteinMPNN (Dauparas et al., 2022) architecture to encode both sequence and structure as model input. The model is trained on the PDB training set used in Dauparas et al. (2022), containing 23,349 protein structures and their ground truth sequences. We first evaluate the effectiveness of the inverse folding model on the PDB test set in Dauparas et al. (2022), which has 1,539 different proteins. As in Nisonoff et al. (2024), we set the temperature during sampling to be 0.1, and randomly sample one sequence conditioned on each structure for both our pretrained discrete flow model and the de facto inverse folding method, ProteinMPNN. As shown in Table 4, the pretrained model performs similarly to ProteinMPNN, achieving comparable sequence recovery rate.

Table 4: Model performance of protein inverse folding on PDB test set.

Method	Sequence Recovery Rate (%) \uparrow
ProteinMPNN	47.9
Discrete Flow Model	48.6

We further evaluate the generalizability of the pretrained model to the proteins in the Megascale dataset. Results on both Megascale training and test set are shown in Table 5. We calculate the self-consistency RMSD (scRMSD) to assess how well a generated sequence folds into the desired structure. Specifically, the generated sequences are folded into 3D structures using ESMFold (Lin et al., 2023), and scRMSD is calculated as their RMSD relative to the original backbone structure we are conditioning on. An scRMSD lower than 2\AA is typically considered a successful inverse folding (Nisonoff et al., 2024; Campbell et al., 2024). As shown in Table 5, the pretrained model achieves a similar sequence recovery rate on Megascale as the PDB test set and low scRMSD, with a success rate greater than 90%, indicating its effectiveness on the inverse folding task.

Table 5: Model performance of protein inverse folding on Megascale proteins.

Eval Dataset	Sequence Recovery Rate (%) \uparrow	scRMSD (\AA) \downarrow	%(scRMSD < 2)(%) \uparrow
Megascale-Train	47.0	0.825	95.0
Megascale-Test	44.0	0.849	90.9

Reward Oracle. We train the reward oracles on the Megascale dataset using the ProteinMPNN architecture initialized with the weights from the pretrained inverse folding model. The oracles take both the protein sequence and the corresponding wild-type structure as input to predict the stability of the sequence, measured by $\Delta\Delta G$ (calculated as the difference in ΔG between the variant and the wild-type from the dataset).

Similar to the practice in the enhancer design experiment, we train two oracles – one for fine-tuning and one for evaluation. The fine-tuning oracle is trained on Megascale training set. We select the best epoch based on validation set performance, and report the Pearson correlation on both Megascale training and test set in Table 6. The performance gap between the training and test sets highlights the difficulty of generalizing to unseen protein structures in this task.

The evaluation oracle is trained on the complete dataset (train+val+test). To attain the best hyperparameters, we randomly split the full dataset into two subsets, an in-distribution set for training, denoted as I, and an out-of-distribution set for validation, denoted as O. Note that here the evaluation oracle is trained part of the variants of *all* wild-type proteins (i.e. Megascale-Train-I & Megascale-Val-I & Megascale-Test-I), and the out-of-distribution set contains unseen sequence variants, but no new structures. The Pearson correlation on each subset is presented in Table 6. It achieves much higher correlations than the fine-tuning oracle, indicating good generalizability of the evaluation oracle to new sequences of in-distribution protein structures. For the final evaluation oracle used to calculate results in Table 2, we train it on the full dataset using the best hyperparameters selected as discussed. It achieves a Pearson correlation of 0.951 on Megascale training set and 0.959 on Megascale test set (both being in-distribution for the evaluation oracle).

Table 6: Performance of the reward oracles for predicting stability conditioned on protein sequence and structure, across a variety of Megascale subsets.

Model	Eval Dataset	Pearson Corr \uparrow
Fine-Tuning Oracle	Megascale-Train	0.828
	Megascale-Test	0.685
Evaluation Oracle	Megascale-Train-I	0.948
	Megascale-Train-O	0.942
	Megascale-Test-I	0.955
	Megascale-Test-O	0.920

Finetuning Setup. We utilize the pretrained inverse folding model and the fine-tuning oracle described above for fine-tuning. During **DRAKES**'s stage 1 data collection, we generate sequences from the pretrained model over 50 steps. We set $\alpha = 0.0003$ and truncate the backpropagation at step 25. The model is finetuned with proteins in Megascale training set with batch size 128 (16 samples per iteration, with gradient accumulated over 8 iterations) for 100 epochs. For **DRAKES** w/o KL, we follow the same setup, but set α to zero. The model is evaluated on Megascale test set, where we generate 128 sequences conditioned on each protein structure for every method (with batch size of 16 over 8 batches) and each random seed. We report the mean and standard deviation of model performance across 3 random seeds.

Evaluation Oracle Accounts for Over-Optimization. As discussed in Section 6.2, for the enhancer design experiment, significant over-optimization occurs when evaluating Pred-Activity, even with an evaluation oracle trained on distinct data unseen during fine-tuning. In contrast, the protein inverse folding experiment largely mitigates this issue. Table 7 shows the median values of Pred-ddG for the generated sequences based on both the evaluation oracle (same as those reported in Table 2) and the fine-tuning oracle. Although **DRAKES** w/o KL shows significantly higher Pred-ddG than **DRAKES**

1242 with the fine-tuning oracle, their performance with the evaluation oracle remains similar, suggesting
 1243 less pronounced over-optimization in evaluation. This is because enhancer sequences are relatively
 1244 homogeneous, and even though we split based on chromosomes, each chromosome still has similar
 1245 regions. However, protein structures are more distinct, and training on different proteins creates
 1246 unique model landscapes.

1247
 1248 Table 7: Model performance on protein inverse folding, with Pred-ddG calculated using either the
 1249 evaluation oracle (Eval) or the fine-tuning oracle (FT).

1250	Method	Pred-ddG-Eval (median) \uparrow	Pred-ddG-FT (median) \uparrow
1251	Pretrained	-0.544(0.037)	0.161(0.012)
1252	CG	-0.561(0.045)	0.158(0.017)
1253	SMC	0.659(0.044)	0.543(0.013)
1254	TDS	0.674(0.086)	0.557(0.005)
1255	CFG	-1.159(0.035)	-1.243(0.013)
1256	DRAKES w/o KL	1.108(0.004)	0.833(0.000)
1257	DRAKES	1.095(0.026)	0.702(0.002)

1258
 1259 **Additional Results.** We provide more examples of the generated proteins in Figure 6, in addition to
 1260 Figure 2. We also provide the specific values for energy, Pred-ddG and scRMSD of the visualized
 1261 protein generated by **DRAKES**, as well as the energy values for the corresponding wild-type structure.
 1262
 1263
 1264
 1265
 1266
 1267
 1268
 1269
 1270
 1271
 1272
 1273
 1274
 1275
 1276
 1277
 1278
 1279
 1280
 1281
 1282
 1283
 1284
 1285
 1286
 1287
 1288
 1289
 1290
 1291
 1292
 1293
 1294
 1295

1296

1297

1298

1299

1300

1301

1302

1303

1304

1305

1306

1307

1308

1309

1310

1311

1312

1313

1314

1315

1316

1317

1318

1319

1320

1321

1322

1323

1324

1325

1326

1327

1328

1329

1330

1331

1332

1333

1334

1335

1336

1337

1338

1339

1340

1341

1342

1343

1344

1345

1346

1347

1348

1349

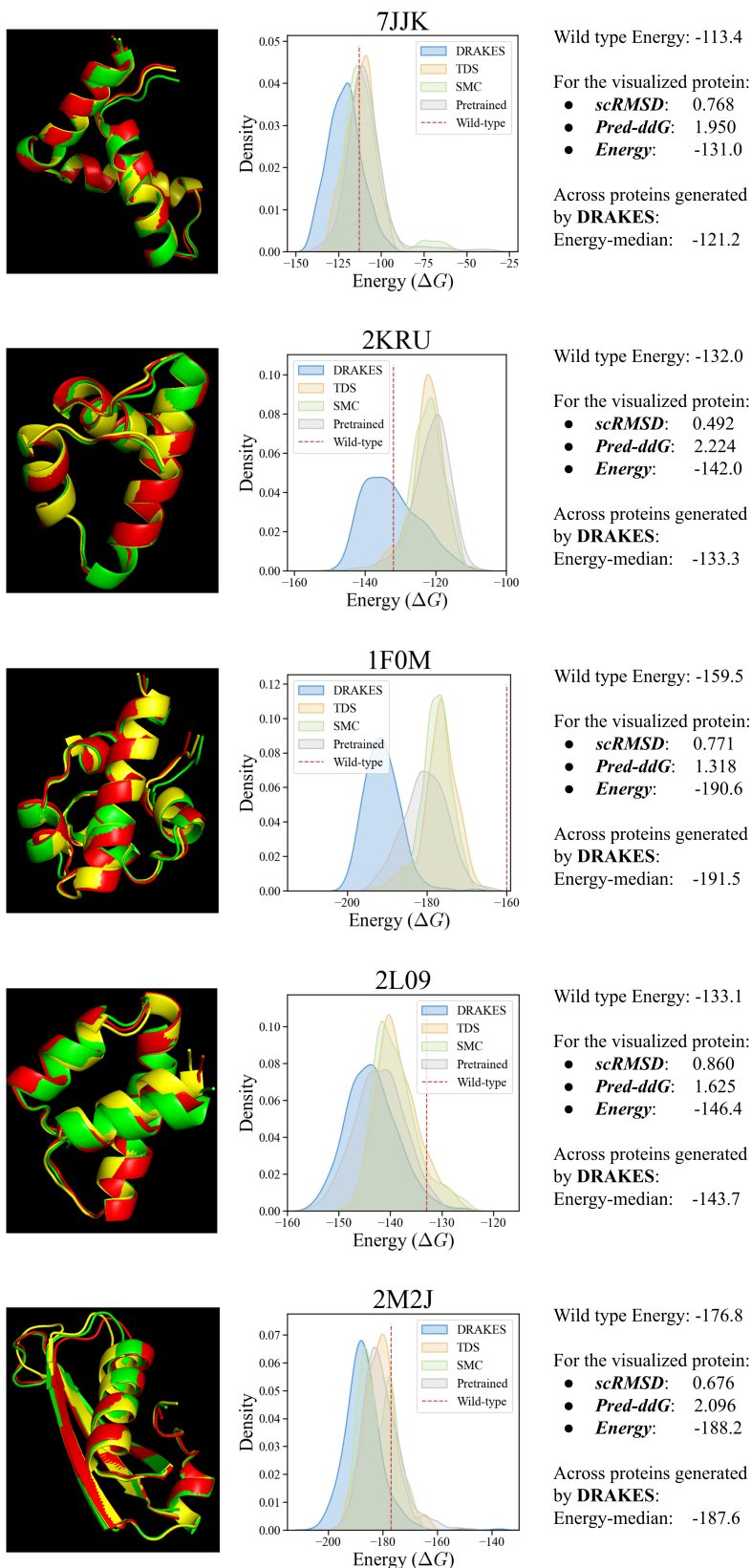


Figure 6: Additional examples of generated proteins.